ELSEVIER

Catalysis Today 50 (1999) 309–328

CATALYSIS TODAY

Characterization of model automotive exhaust catalysts: Pd on ceria and ceria–zirconia supports

H.-W. Jen[a], G.W. Graham[a], W. Chun[a], R.W. McCabe[a,*], J.-P. Cuif[b], S.E. Deutsch[b], O. Touret[c]

[a]*Ford Research Laboratory, Dearborn, MI, USA*
[b]*Rhodia Inc., Cranbury, NJ, USA*
[c]*Rhodia, La Rochelle, France*

Abstract

Pure cerias, silica-doped ceria, ceria–zirconia solid solutions, and ceria–zirconia solid solutions with partial incorporation of praseodymium in the structure were prepared by Rhodia as high-surface-area powders and used as supports in model Pd automotive three-way catalysts prepared at Ford. The catalysts were aged for 12 h at 1050°C, both in air and under redox conditions simulating automotive exhaust gases. Both the fresh and aged catalysts were characterized by a combination of techniques including oxygen storage capacity (OSC) measurements. After aging, catalysts prepared on the solid solution materials provided much greater OSC than those based on pure ceria or silica-doped ceria. Addition of 5 wt% praseodymia as a substitute for ceria improved the thermal stability of the ceria–zirconia, however, without increasing the OSC of the model catalysts. The ceria–zirconia based catalysts revealed a new temperature-programmed reduction peak, between 100°C and 200°C, after 1050°C aging, which is attributed to Pd-assisted bulk reduction of ceria. Significant differences in OSC were noted between catalysts prepared on a series of 70 wt% ceria–30 wt% zirconia supports prepared by different processes, despite virtually identical characteristics of the aged materials as judged by the other techniques. These observations indicate that different processing methods lead to different physical and chemical characteristics of aged catalysts, not readily discerned by conventional characterization techniques, but nonetheless affecting the performance.

Keywords: Catalyst; Ceria; Ceria–zirconia

1. Introduction

Ceria provides a number of benefits in automotive catalysts [1–3], especially oxygen storage – the ability to store oxygen under fuel-lean operating conditions and supply oxygen for converting hydrocarbons (HC) and carbon monoxide (CO) under fuel-rich conditions where gas phase concentrations of oxygen are not sufficient to maintain high conversions. Utilization of ceria in automotive three-way catalysts (TWCs) over the last five years has changed dramatically, with a trend away from alumina-supported ceria to high-surface-area, thermally stable pre-formed powders. Concomitantly, pure ceria has given way to stabilized cerias, most notably ceria–zirconia solid solutions.

*Corresponding author. Present address: Ford Motor Company, Chemical and Physical Sciences Laboratory, Mail Drop 3179, Building SRL, Dearborn, MI 48121-2053, USA. Tel.: +313-337-8042; fax: +313-594-2963; e-mail: rmccabe@ford.com

0920-5861/99/$ – see front matter
PII: S0920-5861(98)00512-4

These developments have led to a new generation of palladium-based TWCs that display excellent thermal stability, even in applications where catalyst temperatures occasionally reach 1000°C [4–7].

Despite these advances, additional stabilization is required to develop TWCs that can withstand even higher temperatures. Applications involving manifold-mounted converters, heavy-duty truck converters, and so-called $\lambda=1$ systems (which avoid the traditional practice of using fuel-enrichment to control exhaust temperatures) can produce catalyst temperatures approaching 1150°C under extreme driving conditions.

The present study represents a collaboration between Ford Motor and Rhodia to investigate the oxygen storage capacities (OSCs) of model Pd-on-ceria (or ceria–zirconia solid solution) catalysts after aging at temperatures up to 1150°C. OSC measurements are supplemented by conventional techniques of catalyst characterization including pore-size measurements by mercury porosimetry, BET surface area measurements, powder X-ray diffraction (XRD), X-ray photoelectron spectroscopy (XPS), and H_2 temperature-programmed reduction (TPR).

2. Experimental

2.1. Catalyst and support materials

All of the ceria and ceria–zirconia solid solution powders were commercially feasible materials supplied by Rhodia. Nominal purity of the ceria and praseodymia used to prepare these materials is 99.5 wt%, with the remaining 0.5 wt% comprised of other rare earth oxides. Nominal purities of zirconia and silica are 98.5 and 99 wt%, respectively. Compositions of the support materials are given in Table 1, expressed as wt% of the respective oxides (CeO_2, ZrO_2, SiO_2, and Pr_6O_{11}). Pure ceria materials are referred to as C1 and C2, the silica-doped ceria as CS, ceria–zirconia materials as CZ1–CZ5, and the ceria–zirconia–praseodymia materials as CZP1 and CZP2.

Model catalysts containing 2 wt% Pd were prepared by impregnation of aqueous solution of Pd nitrate (Alfa) to incipient wetness, followed by drying for 12 h at 55°C and calcination at 600°C for an additional 12 h in a standard muffle furnace.

2.2. Aging protocol

Catalysts were aged both in air and under a laboratory redox cycle designed to simulate air–fuel variations of automotive exhaust. Both redox and air aging were carried out for 12 h at 1050°C; a few samples were also redox aged at 1100°C and 1150°C.

Redox aging was carried out in flowing gases in a tube furnace containing a 3 cm o.d. quartz tube. The powder samples were distributed as thin layers in quartz boats inserted into the tube. The gas mixture contained 1 mol% CO/H_2 ($[CO]/[H_2]=3/1$) alternating every 10 min with 0.5 mol% O_2; the remainder of the mixture consisted of 0.002 mol% SO_2, 10 mol%

Table 1
XRD characteristics of fresh and aged (1050°C/12 h) oxides

Designation	Composition (wt%) $CeO_2/ZrO_2/Pr_6O_{11}$	Lattice parameter (nm)		Calculated wt% ZrO_2 (from XRD)	
		Fresh	Aged in: air (redox)	Fresh	Aged in: air (redox)
C1	99.5/0/0	0.541	0.541 (0.5413)	0	0 (0)
C2	99.5/0/0	0.540	0.541 (0.5409)	0	0 (0)
CS	99.2/0.8 (SiO_2)	0.540	0.541 (0.5411)	0	0 (0)
CZ1	90/10/0	0.539	0.538 (0.5376)	5.0	7.7 (11.9)
CZ2	70/30/0	0.532	0.536[a] (0.5311)	24.5	13.0 (34.4)
CZ3	70/30/0	0.531	0.536[a] (0.5309)	27.6	13.0 (35.1)
CZ4	70/30/0	0.531	0.536[a] (0.5309)	27.6	13.0 (35.1)
CZ5	70/30/0	0.532	0.535[a] (0.5311)	24.5	15.8 (34.4)
CZP1	66.5/28.5/5.0	0.533	0.533 (0.5316)	na	na (na)
CZP2	66.5/28.5/5.0	0.534	0.534 (0.5314)	na	na (na)

[a]Lattice parameter of main cubic phase.

H_2O, and balance N_2 (total flow rate=5 l/min). The redox aging ended with the oxidizing portion of the cycle, followed by 30 min of natural cooling in flowing N_2 to about 500°C. The N_2 flow was then stopped and the sample was cooled to room temperature with the outlet of the tube open to air.

2.3. Surface area measurements

The specific surface areas of the powders were determined by the BET method in a Micromeritics Gemini 2360 surface area analyzer. Samples were degassed under flowing inert gas at 250°C for at least 30 min before measurement. The estimated error in the measurement is 5% (relative).

2.4. Pore volume measurements

Pore volume distributions were measured by mercury intrusion and calculated with the Washburn equation on a Micromeritics Autopore 9410 instrument. The lower pore diameter limit on this instrument is 3 nm. A filling pressure of 2 psi was used, leading to an upper pore diameter limit of 100 000 nm. Samples were dried in air at 110°C for at least 1 h before intrusion measurements were performed. Porosimetry measurements were performed on powders before impregnation with Pd and on Pd model catalysts after redox aging at 1050°C for 12 h.

2.5. X-ray diffraction

Powder XRD data were obtained both at Ford and at Rhodia. The Ford measurements were performed with a Scintag X1 diffractometer, in θ/θ orientation, using Cu K_α radiation. The samples were held in a cylindrical cavity, 9 mm in diameter and 0.5 mm deep, cut into the surface of a zero-background quartz plate. The Rhodia measurements were performed with a Siemens GADDS Hi-Star diffractometer using Co K_α radiation. Samples were mounted by dusting a thick layer of the powder onto double sided tape stuck to an aluminum sample holder.

2.6. Hydrogen temperature-programmed reduction

TPR experiments were carried out with an Altamira system employing a thermal conductivity detector. The standard pretreatment involved heating the powder sample (typically 100 mg) for 1 h in flowing 10% O_2 in He at 500°C to ensure full oxidation. The sample was then cooled to room temperature (in static 10% O_2/He) and further cooled to −50°C in Ar. After switching to a feed of 9.4% H_2 in Ar, the TPR trace was acquired by ramping from −45°C to 900°C at a rate of 10°/min. Hydrogen consumption (μmol H_2 per gram of sample) was quantified by integrating the areas under the peaks, utilizing sensitivity factors measured after each run (from injection of known quantities of the 9.4% H_2/Ar gas mixture). No curve fitting was employed; integrations involved simply calculating the area under the curve over a selected temperature range.

2.7. X-ray photoelectron spectroscopy measurements

Surface characterization was performed by XPS with a Surface Science Instruments photoelectron spectrometer coupled to a Physical Electronics reactor. Samples for the XPS measurements were prepared by pressing pellets from powder which had previously been aged. In order to accelerate outgassing and remove C from the surface, samples were heated at 500°C for 4 h in flowing O_2 before being transferred, under vacuum, to the spectrometer. A survey spectrum and the relevant core-level spectra (generally the most intense from each element) were then acquired under computer control. The survey spectra were checked to see that the sample surfaces were relatively free of C (i.e., had less than a few at%) and that no unexpected elements were present. Normalized surface compositions were computed on a metals basis, in the usual way, without making corrections for differences in the photoelectron inelastic mean free path between the various core levels used.

2.8. Oxygen storage capacity measurements

Oxygen storage measurements were carried out in a flow reactor system, designed for powder samples, equipped with solenoid valves for rapid introduction of step pulses of CO and O_2. Catalyst samples were prepared by pressing thin disks from powders and breaking the disks into small pieces. The fragments were loaded into a 0.4 cm i.d. quartz u-tube reactor

jacketed by a heater coil of nichrome wire. A total gas flow rate of 500 std. cm^3/min was employed through a catalyst bed typically 2.2 cm in length, yielding a pressure drop of about 3.5 kPa (∼0.5 psi) at room temperature.

An overall system response time of 0.6 s (from valve actuation to detection of the steady-state signal at the UTI 100C quadrupole mass spectrometer) was achieved by locating miniature fast-response solenoid valves just before the inlet to the reactor and utilizing 0.016 cm (1/16 in.) o.d. stainless steel tubing for all transfer lines between the solenoid valves and mass spectrometer.

Prior to an OSC measurement, the sample was first heated in 0.5% O_2/He at 500°C for at least 20 min. The sample was then exposed to 0.5% O_2 and 1% CO pulses (both in He carrier) at the desired test temperature. Most of the OSC data reported here involved relatively long cycles consisting of 25 s in O_2 followed by 50 s in CO with a 10 s pulse of He in-between to ensure complete flushing of gas phase species between pulses. A few experiments were carried out with alternating 10 s pulses of CO and O_2 with 10 s of He in-between. Ar was injected along with the CO pulse and was used as an internal standard for quantification of gas concentrations. The mass spectrometer was used to monitor CO (mass 28), O_2 (mass 32), Ar (mass 40) and CO_2 (mass 44) at 0.2 s intervals during each experiment. Corrections were made to the mass 28 and 32 signals due to cracking of CO_2.

OSC was quantified in terms of micro-moles of oxygen atoms per gram of catalyst (μmol O/g) by comparing integrated amounts of CO in the pulses entering and exiting the reactor. Close agreement was obtained between oxygen uptakes calculated from consumption of CO and those calculated from either production of CO_2 or consumption of O_2 (during re-oxidation of the catalyst).

3. Results

3.1. Phase identification

3.1.1. Fresh materials

Fig. 1(a) shows representative XRD patterns for the fresh model catalysts, all of which are characteristic of the cubic (calcium fluoride) structure of ceria, shifted and/or broadened to various extents reflecting differences in composition and crystallite size. No evidence of Pd is obtained in any of the fresh materials, indicating small particles of PdO with mean diameters less than 5 nm. The catalysts supported on ceria or nearly pure ceria have cell parameters near the theoretical value of 0.541 nm for ceria as summarized in Table 1 (CZ1, containing 10% zirconia, is shifted slightly to 0.539 nm). In contrast, the catalysts on the 70/30 CZ and CZP supports show much larger shifts in peak position, and correspondingly smaller cell parameters (Table 1), as expected given the smaller effective ionic radius of Zr^{4+} (0.084 nm) compared to Ce^{4+} (0.097 nm). The measured cell parameters were used to estimate the amount of ZrO_2 in solid solution by applying an empirical Vegard-type rela-

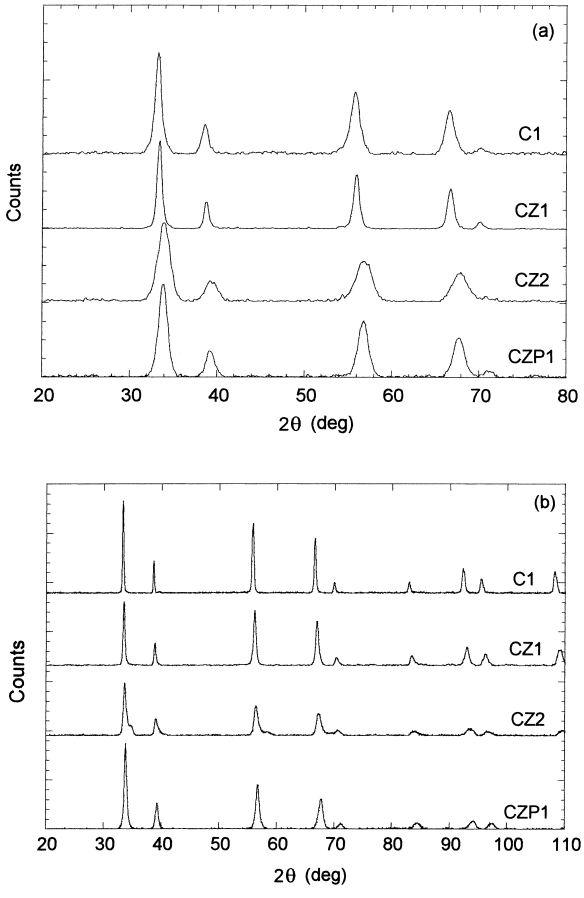

Fig. 1. XRD patterns (Co K_α source) of representative fresh (a) and 1050°C air aged (b) oxide materials (loaded with 2 wt% Pd).

tionship for solid solutions developed by Kim [8]. For the 70/30 CeO_2/ZrO_2 materials, the accuracy of the calculation is estimated at ±3%. Thus, samples CZ3 and CZ4 appear to be essentially single phase solid solutions as prepared, while samples CZ1, CZ2, and CZ5 contain at least one other amorphous or crystalline phase. XRD, however, revealed no phases other than the cubic fluorite phase for any of the fresh ceria–zirconia materials.

3.1.2. Aged catalysts

Fig. 1(b) shows XRD patterns of representative model catalysts after air aging at 1050°C for 12 h. Compared to the fresh samples, all peaks are sharper indicating larger crystalline domains. The catalysts made from pure or essentially pure ceria (e.g., C1 and CZ1) retain the cubic structure with no evidence of other phases (except PdO), as do those made from the CZP materials (e.g., CZP1). In contrast, the 70/30 CZ aged catalysts, as represented by sample CZ2 in Fig. 1(b), reveal broadening and splitting of peaks characteristic of a second phase with smaller cell parameter. The main (ceria-rich) phase can only account for 45–55% of the Zr in these samples (as shown by the calculated wt% ZrO_2 data in Table 1). Thus, 1050°C air aging produces phase segregation resulting in a second, zirconia-rich, cubic or tetragonal phase, consistent with published data [9].

XRD patterns were also obtained for the 1050°C redox-aged catalysts. Results are generally consistent with those observed after air-aging except that no phase segregation is observed for the 70/30 CZ supports. This can be seen in Fig. 2 by the close correspondence between diffraction patterns of the zirconia-containing materials and that of pure ceria (C1). Also, lattice parameters of the redox aged samples (Table 1) are close to those of the fresh samples. The 70/30 CZ materials, in particular, yield calculated ZrO_2 concentrations close to theoretical for a homogeneous solid solution, in contrast to their air-aged counterparts.

Samples of 1050°C (or 1150°C) redox aged catalysts were oxidized in air at 700°C for 2 h (conditions known to completely convert Pd to PdO) and then re-examined by XRD over the range of the Pd(1 1 1) and PdO(1 1 0) reflections (near 40° and 42°, respectively, for Cu K_α radiation). The data are summarized in Fig. 3. All of the samples show prominent PdO(1 1 0) features with peak widths characteristic of particle diameters greater than 10 nm (the CZ2–CZ5 samples also have a weak CZ diffraction feature at ~41.75°). However, some of the samples (C1, C2, CS, and, to a

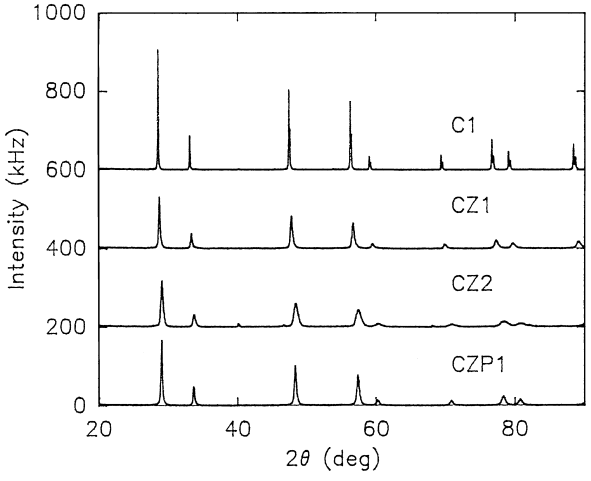

Fig. 2. XRD patterns (Cu K_α source) of representative oxide materials (loaded with 2% Pd) after redox aging at 1050°C. Note the absence of any features characteristic of tetragonal zirconia in the patterns for the zirconia-containing materials.

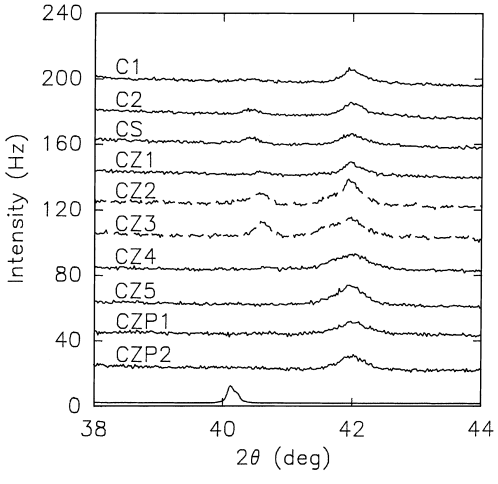

Fig. 3. XRD patterns (Cu K_α source) of 1050°C (or 1150°C – dashed lines) redox aged materials (loaded with 2% Pd) after 2 h, 700°C oxidation in air. The pattern is obtained over the range of the Pd(1 1 1) reflection (40–41°) and the PdO(1 1 0) reflection (42°). The solid curve at the bottom of the figure was obtained on fully reduced 2% Pd on a CZ support (after redox aging at 1050°C) and is displayed at 1/10 the scale of the other traces.

lesser extent, CZ1) reveal a Pd(1 1 1) peak, but it is shifted to slightly larger scattering angle than normal (compare with reference pattern at the bottom of Fig. 3). Normally, metallic Pd would not be expected after the 700°C oxidation. However, both the presence of metallic Pd and the slight shift of the diffraction peak has been observed previously for similar materials [10] and is attributed to a deep physical encapsulation of Pd particles under tremendous compressive force by the ceria. The amount of encapsulated Pd is small after 1050°C aging, amounting to no more than 5% of the Pd. Redox aging of the Pd/CZ2 and Pd/CZ3 catalysts at 1150°C increased the amount of encapsulated Pd to about 10% at most (dashed curves). Application of the Scherrer relation to the Pd(1 1 1) diffraction peak in redox-aged catalysts (following a mild reduction in 1% H_2 at 500°C for 0.5 h) indicates that the Pd particles are about 40 nm in diameter.

3.2. *Physical characteristics (surface area and pore volume distribution)*

3.2.1. *BET surface area*

BET surface area data of both fresh and aged samples (loaded with 2% Pd) are presented in Table 2. Fresh BET areas range from 46 to 114 m^2/g with most of the samples at 83±5 m^2/g. No trends are observed with composition of the oxide supports, and the differences in BET areas primarily reflect differences in synthesis methods.

Aging for 12 h at 1050°C in either air or under redox conditions leads to considerable loss of area – more than an order-of-magnitude in many cases.

Table 2
BET surface areas of oxide materials loaded with 2 wt% Pd

Designation	BET surface area (m^2/g)		
	Fresh	1050°C air	1050°C redox
C1	114	3	1
C2	81	11	4
CS	82	19	4
CZ1	54	3	6
CZ2	78	7	7
CZ3	79	5	7
CZ4	46	7	8
CZ5	87	9	7
CZP1	86	8	8
CZP2	87	14	10

Although the data in Table 2 are presented for samples which contain 2% Pd, experiments on samples without Pd give essentially identical results. Major observations include:

1. pure or nearly pure ceria supports show the greatest loss of surface area (especially under redox conditions),
2. BET areas of the 70/30 CZ supports all lie between 5 and 9 m^2/g, regardless of aging environment,
3. the most stable materials are the CZP supports, with BET areas of 8–14 m^2/g, and
4. the CS material retains the greatest surface area in air (19 m^2/g), but shows poor stability in redox environments (4 m^2/g), most likely because of the steam present in the redox gas mix.

The large surface area loss caused by redox aging of the CS material is consistent with photoemission evidence (see Section 3.4) indicating virtually complete segregation of SiO_2 and CeO_2.

The pure cerias (C1 and C2) retain less surface area after redox aging than after air aging, while the CZ and CZP materials give mixed results, with no obvious trend as a group toward greater surface area stability under one aging condition as compared to the other.

3.2.2. *Porosimetry data*

Table 3 contains cumulative pore volume and median pore diameter data for the fresh support materials (before impregnation) and for the redox-aged model catalysts. The median pore diameter is based on the median surface area of the samples (i.e., half of the surface area accessible to mercury is found in pores larger (or smaller) than the median pore diameter).

Most of the samples display two or three step-like intrusions of mercury with increasing pressure (i.e., decreasing pore diameter). Representative examples are shown in Fig. 4 for the fresh and redox-aged CZ3 and CZP2 materials. The pore diameter regime of greatest interest is below 1000 nm which represents filling of the mesopores of the powder particles. For CZ3, this occurs in two distinct steps, the first around 1000 nm and the second around 10 nm. CZP2, in contrast, shows only one step in the mesoporous region – between 100 and 10 nm.

Redox-aging increases the median pore diameter and decreases the cumulative pore volume (except for CS) compared to the fresh materials. Pore volume

Table 3
Cumulative pore volumes (3–100 000 nm pores) and median pore diameter determined by Hg intrusion

Sample	Cumulative pore volume (ml/g)		Median pore diameter (nm)	
	As-prepared	Redox aged	As-prepared	Redox aged
C1	0.54	0.21	5	330
C2	0.48	0.31	8	75
CS	0.45	0.47	8	120
CZ1	0.41	0.21	12	45
CZ2	0.63	0.32	11	57
CZ3	0.63	0.31	10	39
CZ4	0.61	0.33	14	41
CZ5	1.11	0.43	18	87
CZP1	0.56	0.29	8	38
CZP2	1.07	0.46	18	69

losses occur across the full range of pore sizes, but the loss is greatest in the mesoporous region below 1000 nm as can be clearly seen by comparing the traces for the fresh and aged materials in Fig. 4. Except for CS, the fresh samples with the largest pore volumes retain the largest pore volumes after redox aging. The pore volume distribution primarily reflects the specific process by which the oxide materials are prepared rather than the composition.

3.3. Reducibility (from H_2-TPR)

3.3.1. Blank supports

Pure ceria (C2), in the fresh state, gives the typical dual-peak TPR signature (Fig. 5(a)) attributed to 'surface' (peak near 500°C) and 'bulk' (peak near 800°C) reduction [3,11]. After redox aging at 1050°C (Fig. 5(a)), only a trace of the low-temperature reduction feature remains, consistent with the 20-fold loss of surface area. The fresh ceria–zirconia oxides, in contrast, show a main reduction peak between 500°C and 600°C with a plateau extending to high temperatures (Fig. 5(b)). Unlike pure ceria, where the low-temperature peak disappears after high-temperature aging, the low-temperature peak of the solid solution sharpens and remains large despite an order-of-magnitude loss in surface area (Fig. 5(b)).

Reduction of the solid solution involves simultaneous surface and bulk reduction between 450°C and 650°C, at rates largely independent of particle size or degree of crystallinity (as indicated by the similar reduction characteristics of fresh and aged samples). A similar concurrence of bulk and surface reduction has been reported by Fornasiero et al. [12] for a $Ce_{0.5}Zr_{0.5}O_2$ mixed oxide, thus suggesting a common rate limiting step. Balducci et al. [13] have carried out calculations which indicate that surface Ce(IV)/Ce(III) reduction energies in the mixed oxides are comparable to bulk values which, in turn, are significantly lower than those in pure ceria [14]. Hori et al. [15] have also pointed out the importance of oxygen transport in the surface region – noting that bulk oxygen diffusivity is not rate-limiting, either for pure ceria or the mixed oxides, and suggesting that the controlling feature is the ability of the mixed oxides to undergo deeper reduction without experiencing phase changes that inhibit the insertion of oxygen vacancies into the surface.

3.3.2. Pd-loaded supports

Fig. 6 shows a TPR trace for the fresh Pd/C2 catalyst. In contrast to blank ceria, no evidence of the 500°C peak remains and a new feature appears below 100°C. Reduction of bulk ceria near 800°C is still evident. The low temperature feature is partly due to reduction of PdO and partly due to reduction of ceria, as evidenced by the fact that the H_2 uptake below 300°C (460 μmol/g – Fig. 7) is close to the sum of the theoretical value of 188 μmol/g (attributable to reduction of PdO alone) and ca. 300 μmol/g from the ''surface'' oxygen in pure ceria (i.e., the peak at 500°C for fresh C2 in Fig. 5(a) is shifted down to below 100°C).

The TPR characteristics of the fresh CZ(P) supported catalysts (e.g., Pd/CZ3 in Fig. 6) are similar to those of the (nearly) pure cerias; reduction of ceria

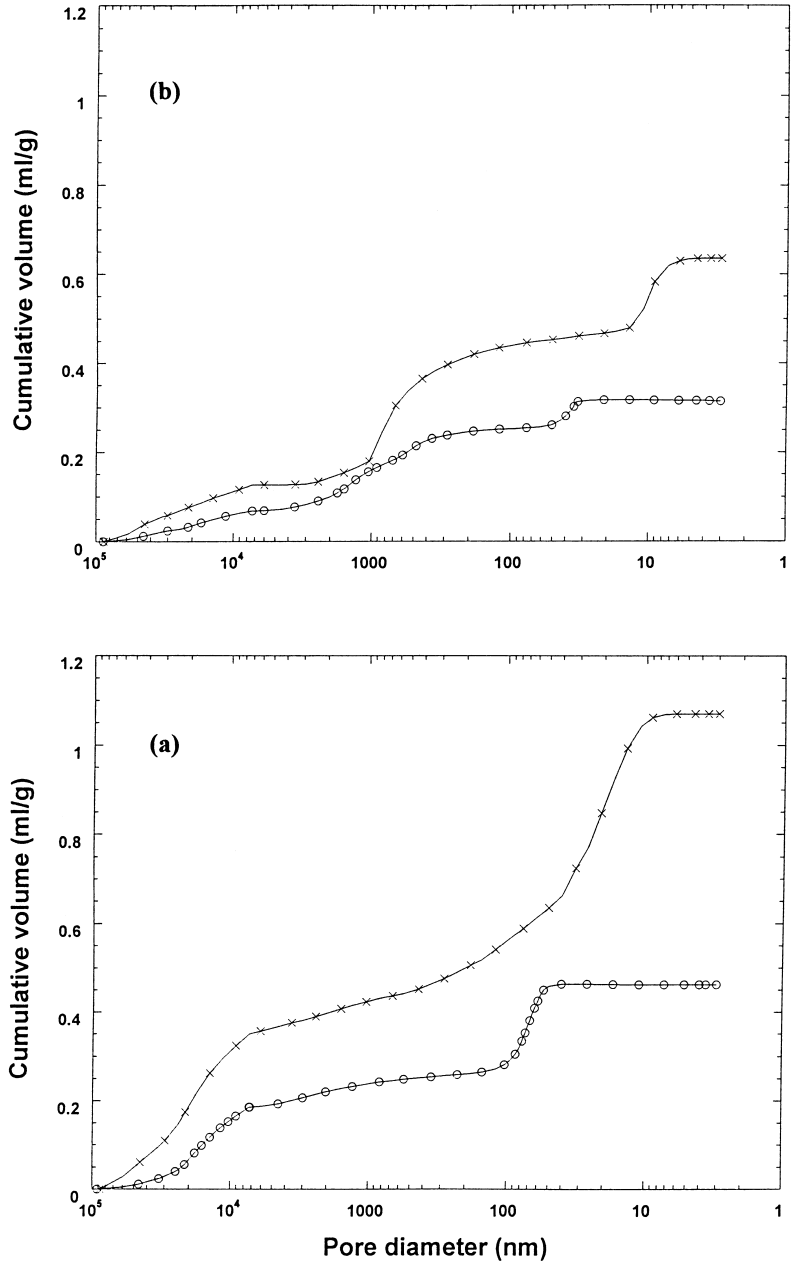

Fig. 4. Pore size distributions of fresh powders (– × –) and redox aged model catalysts (– ○ –): (a) CZP2 and (b) CZ3.

occurs in tandem with reduction of PdO below 100°C. As quantified in Fig. 7, the H_2 uptakes of the Pd/CZ(P) catalysts below 300°C are greater than those of the Pd/C(S) catalysts, indicating greater contribution of oxygen from the support.

Redox aging at 1050°C produces significant changes in the reduction characteristics of Pd on both the ceria and solid solution supports. Fig. 8 shows representative TPR traces for 2% Pd on the C2 and CZ3 supports. All of the aged Pd-containing catalysts

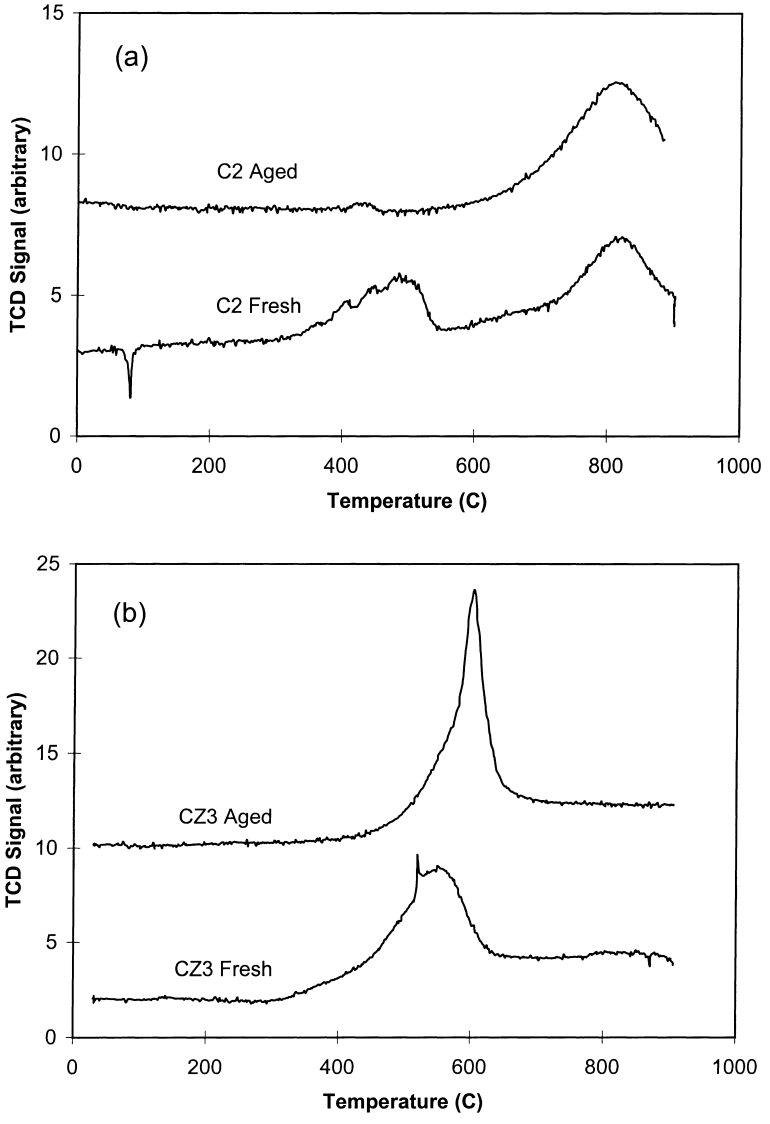

Fig. 5. TPR traces of fresh and 1050°C redox aged (a) C2 (100% CeO_2) and (b) CZ3 (70% CeO_2/30% ZrO_2) material.

display a negative peak near 75–80°C which is also seen in the reduction of bulk PdO and has been attributed to decomposition of Pd hydride [16]. Splitting is observed in the low-temperature PdO reduction peak of the 1050°C redox aged catalysts in Fig. 8. However, this was also seen in fresh samples in some cases, and is attributed to variations in sample packing characteristics and slight run-to-run variations in the heating ramp (integrated H_2 uptakes are quite reproducible, however). All of the aged catalysts are characterized by loss of H_2 area in the low-temperature peaks (i.e., below the hydride decomposition temperature). The remaining H_2 uptake is indicated by the bars designated BH in Fig. 7 and is less than or equal to theoretical for PdO reduction alone (horizontal line in Fig. 7), implying little or no contribution from ceria.

The most significant difference between the C(S) and CZ(P) supported catalysts after aging is the

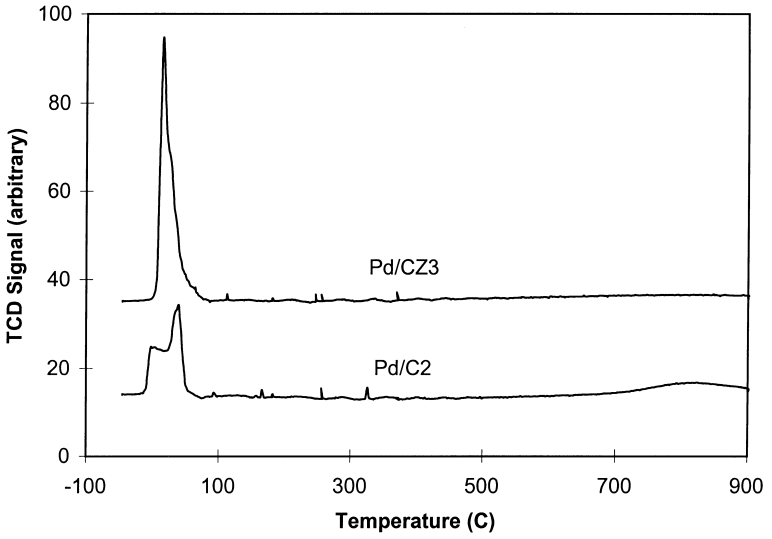

Fig. 6. TPR traces of fresh 2 wt% Pd on C2 (100% CeO_2) and CZ3 (70% CeO_2/30% ZrO_2) catalysts.

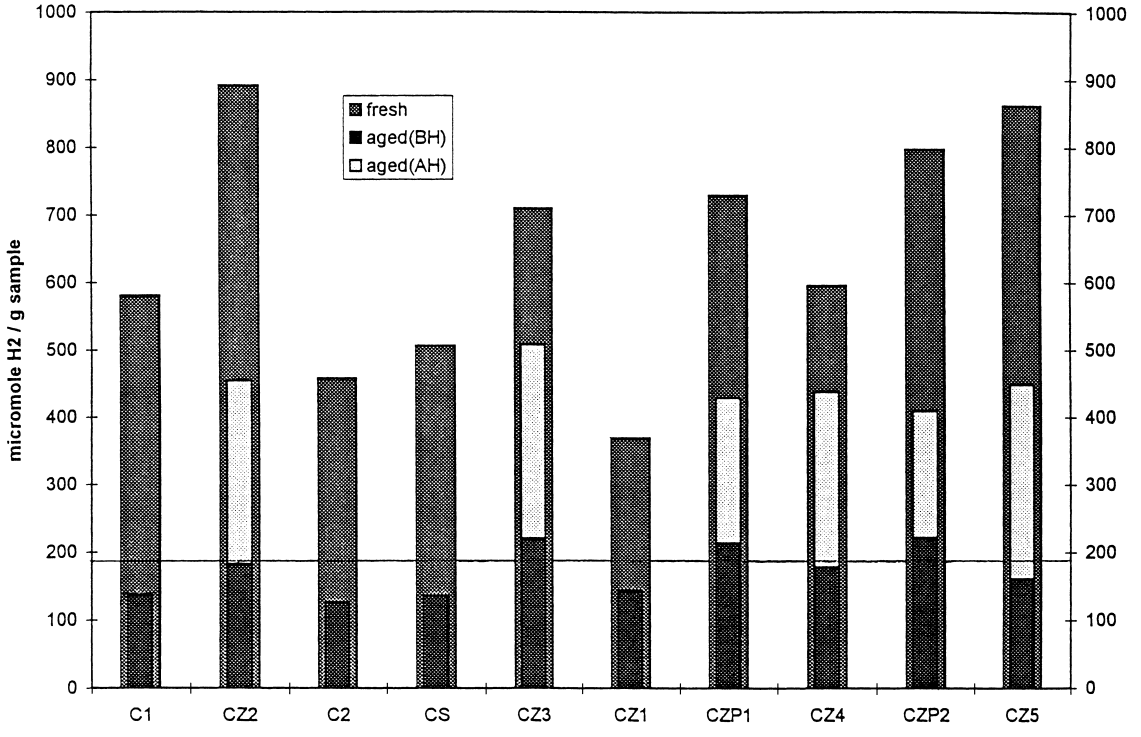

Fig. 7. Integrated H_2 uptakes in the low-temperature regime (<300°C) for fresh and 1050°C redox aged samples of 2% Pd on the various support materials. For the aged materials, the uptakes are broken out into two parts – one below the negative hydride decomposition peak near 80°C (solid bars – BH), and the other above the hydride feature (open bars – AH). The horizontal line at 188 μmol H_2/g sample represents the theoretical H_2 consumption for complete reduction of 2% Pd (as PdO).

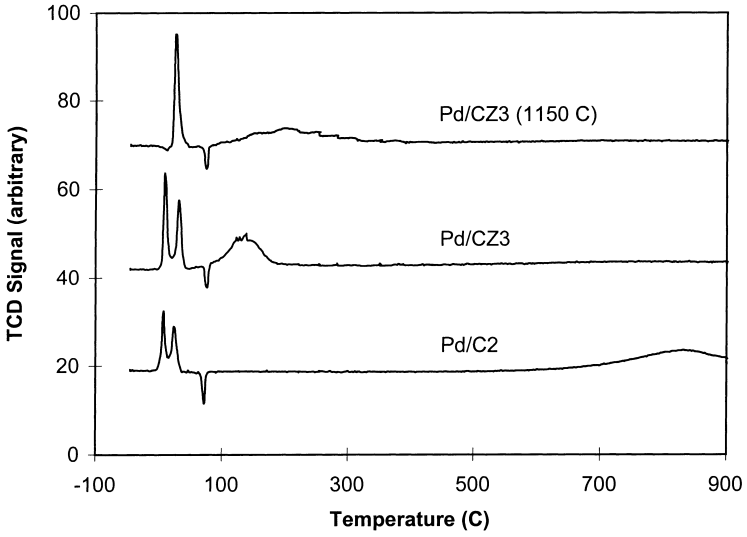

Fig. 8. TPR traces of 1050°C redox-aged 2% Pd on C2 (100% CeO_2) and CZ3 (70% CeO_2/30% ZrO_2) catalysts and 1150°C redox-aged 2 wt% Pd on CZ3 (70% CeO_2/30% ZrO_2) catalyst.

appearance of a new TPR feature between 100°C and 200°C for the CZ(P) supported catalysts. XRD analysis of similar Pd/CZ catalysts, obtained after interrupting the TPR scan at 80°C, indicates that PdO is reduced prior to the appearance of the new feature. Thus, the new peak is due to reduction of Ce(IV) to Ce(III), but at much lower temperature than on the blank supports. Pd still facilitates reaction between H_2 and CeO_2 in the solid solution after aging, although not as effectively as in the fresh catalyst. Most importantly, the peak between 100°C and 200°C contributes significantly to the total H_2 uptake in the temperature regime below 300°C, accounting for more than half in most cases (compare BH and AH bars in Fig. 7).

The temperature of the second reduction peak provides an indication of the severity of aging for a particular material. The top curve in Fig. 8 is the TPR trace for the 2% Pd/CZ3 catalyst after 1150°C redox aging. Compared to the same catalyst after 1050°C aging, the second feature is broader and its peak is shifted upward by 50–200°C. Air aging at 1050°C also produces the second feature between 100°C and 200°C. However, its integrated area is smaller than that of the corresponding redox-aged catalyst (e.g., 170 vs. 285 μmol/g for Pd/CZ3 and 165 vs. 250 μmol/g for Pd/CZ4).

3.4. Surface characterization by XPS

Results of the XPS measurements following redox aging are shown in Table 4. The data are presented as atom % of the metals, uncorrected for differing escape depths of photoelectrons from the different elements. (The column labeled A_s is just the BET surface area, taken from Table 2.) The multiple entries, arising from two distinct measurements made at different points on the same sample, provide an indication of measurement variability. Due to the uncertainty in converting these data to actual surface composition, we focus on relative comparisons of surface concentrations between the various samples, and restrict our discussion of surface segregation to broad observations only.

Considering the [Pd]'s as a whole, it is clear that there are significant variations amongst the samples. Probably the main reason for this is the variation in specific surface area, A_s, since the areal density of Pd on the support surface must increase as the oxide support undergoes sintering. Within the set of 70/30 ceria–zirconia materials, CZ2-5, the surface area is fairly constant, between 7 and 8 m^2/g, and yet there still appears to be a significant difference in [Pd] between CZ2 and CZ3, on the one hand, and CZ4 and CZ5, on the other. This may indicate a real

Table 4
Apparent surface compositions (i.e., uncorrected for differing escape depths of photoelectrons from the different elements), as atom % of the metals, of redox-aged catalysts

	[Pd]	[Ce]	[Si]	[Zr]	[Pr]	A_s (m^2/g)
C1	6.4	93.6				1
	5.1	94.9				
C2	4.2	95.8				4
	3.8	96.2				
CS	3.8	68.2	28.0			4
	3.1	63.3	33.6			
CZ1	4.1	74.1		21.8		6
	3.1	74.4		22.5		
CZ2	2.3	50.7		47.0		7
	2.4	50.5		47.1		
CZ3	2.0	48.5		49.5		7
	2.0	48.4		49.6		
CZ4	0.9	47.7		51.4		8
	1.4	49.7		48.9		
CZ5	1.1	50.0		48.9		7
	1.3	50.8		47.9		
CZP1	1.5	45.0		46.4	7.1	8
	1.5	43.5		48.2	6.8	
CZP2	1.4	44.7		47.3	6.6	10
	1.2	44.9		47.2	6.7	

difference in Pd dispersion, since [Pd] should be proportional to Pd dispersion, as shown in Appendix A.

The high [Si] of CS after aging (compared with the almost zero [Si] of fresh CS) indicates essentially complete segregation of ceria and silica. Other XPS measurements performed in our laboratory on a similar mixed oxide have provided evidence of such segregation after redox aging at temperatures as low as 600°C. The same behavior was also observed after air aging, but higher temperatures were required in order to attain the same degree of segregation.

On the other hand, there is no such evidence for segregation of ceria and zirconia upon aging, the [Ce]'s and [Zr]'s of aged catalysts remaining basically the same as those of the fresh. The [Ce]/[Zr] ratios in Table 4, at first sight too low, are consistent (to a first approximation) with the nominal bulk compositions of the mixed oxides if the difference in sampling depth due to the difference in inelastic mean free path between the Ce-3d and Zr-3d photoelectrons is taken into account. The [Pr]/[Ce] ratio for both the CZP1 and CZP2 catalysts is about 50% too high, however, and there should be little difference in sampling depth in this case. A possible explanation can be constructed, based on the premise that most of the Pr is contained in relatively small domains of praseodymia–zirconia where Pr exists in the +3 oxidation state. The spectra in Fig. 9, which show that the Pr in these two samples is indeed less than fully oxidized, further support the suggestion that Pr is not in intimate contact with Ce in these mixed oxides [17]. Consequently, praseodymia would not be expected to contribute to the oxygen storage capacity of these catalysts.

3.5. Oxygen storage characteristics

3.5.1. Oxygen storage capacities

Table 5 summarizes oxygen storage capacities, measured in long-pulse (50 s) CO titration experiments, for selected materials (blank or with 2% Pd). Fig. 10 shows a typical pulse sequence over a catalyst under non-reactive conditions (23°C). The blank data can be compared with data shown in Fig. 11 for the fresh C2 and CZ3 materials (without Pd) at 500°C. As evident from the areas under the CO_2 traces beginning near 40 s, OSC is low in both cases, but more so for the C2 material than for the CZ3 material (for which CO_2 production persists over the full 50 s of the CO pulse).

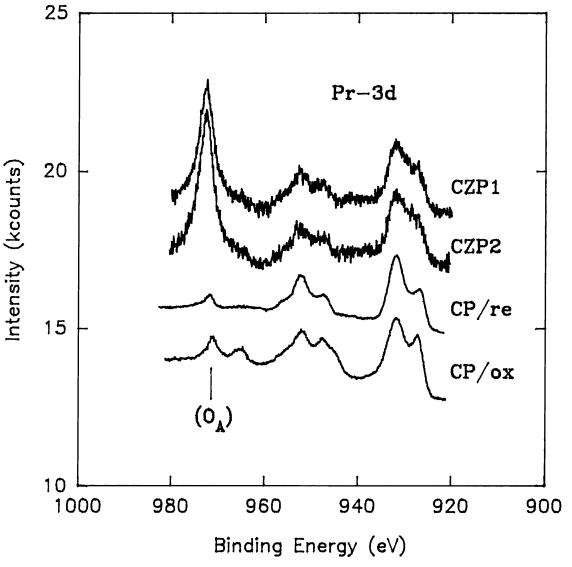

Fig. 9. Pr-3d core-level spectra from Pd/CZP1, Pd/CZP2, and both reduced and oxidized samples of a homogeneous ceria–praseodymia solid solution (labeled CP/re and CP/ox, respectively), showing that Pr in the CZP samples is not fully oxidized [17]. (The feature labeled O_A is due to an O Auger transition.)

Addition of Pd dramatically increases OSC, as evident in Fig. 12 which presents corresponding data for the same materials loaded with 2% Pd. Both catalysts demonstrate a plateau in CO_2 production following introduction of CO which indicates complete consumption of the CO. As with the blank supports, the catalyst prepared on the CZ3 material displays better OSC characteristics than that on the C2 material, both in its overall OSC (965 vs. 364 μmol O/g) and in its ability to preserve complete CO consumption for longer time (17 vs. 7 s). The differences in OSC between samples with and without Pd decreases, however, as the evaluation temperature is increased. This can be seen in the data of Table 5 for the fresh C2 and CZ3 materials; in each case, OSC at 700°C increases only slightly with addition of Pd.

Integrated OSC values of all the catalysts containing 2% Pd (with the exception of the C1 material) were measured after 1050°C redox aging (and also after air aging for CZ3 and CZ4) and are reported in Table 5. A few trends are evident in the table: (1) aging dramatically decreases the amount of stored oxygen compared to the fresh catalysts (cf. C2 and CZ3 data), (2) air aging decreases OSC more than redox aging, which can be related to the difference in phase stability (cf. CZ3 and CZ4), and (3) among the 1050°C redox aged Pd-containing catalysts, two of the four supported on 70/30 ceria–zirconia (CZ3 and CZ4) yield the highest OSC at 350°C (570 and 500 μmol O/g, respectively); in order of decreasing

Table 5
Oxygen storage capacities (μ mol O/g cat.) evaluated at 350°C, 500°C, and 700°C

Support	Catalyst/aging	350°C	500°C	700°C
C2	Blank/600 (air)	100	210	300
	2% Pd/600 (air)	270	360	370
	2% Pd/1050 (redox)	4	50	120
CS	2% Pd/1050 (redox)	25	100	140
CZ1	2% Pd/1050 (redox)	300	430	590
CZ2	2% Pd/1050 (redox)	390	620	810
	2% Pd/1150 (redox)	90	390	600
CZ3	Blank/600 (air)	140	590	960
	2% Pd/600 (air)	890	970	1030
	2% Pd/1050 (air)	350	624	686
	2% Pd/1050 (redox)	570	680	880
	2% Pd/1100 (redox)	510	670	900
	2% Pd/1150 (redox)	240	510	720
CZ4	2% Pd/1050 (air)	315	642	709
	2% Pd/1050 (redox)	500	780	870
CZ5	2% Pd/1050 (redox)	460	720	930
CZP1	2% Pd/1050 (redox)	460	660	880
CZP2	2% Pd/1050 (redox)	460	720	930

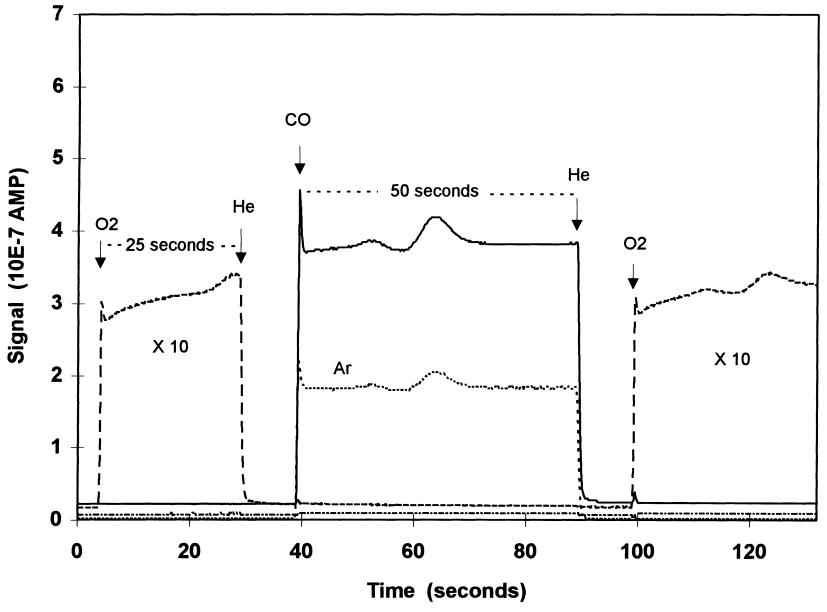

Fig. 10. Typical pulse sequence in OSC measurement (obtained at 23°C under non-reactive conditions).

OSC they are followed by the catalysts supported on CZ5 and CZP (460 μmol O/g), CZ2 (390 μmol O/g), the 90/10 CZ (300 μmol O/g), and the essentially pure cerias (≤25 μmol O/g).

In addition to the large differences in OSC effected by the different support compositions, large variations are also observed among supports with nominally the same composition. Within the group of four catalysts supported on 70/30 CZ, e.g., OSC (at 350°C) ranges from 570 μmol O/g for CZ3 to 390 μmol O/g for CZ2. Fig. 13 contains a comparison of OSC traces for the two catalysts. The difference in OSC arises from different initial rates of CO_2 production; on CZ3 the initial rate is sufficient to convert all of the CO for 2–3 s before starting to fall, whereas on CZ2 a monotonic decrease in rate is observed immediately upon switching to CO. Thus, kinetics of the reaction between CO and stored oxygen play a large role in defining the best OSC materials. This is further borne out by cycling experiments conducted with 10 s pulses of CO and O_2, shown in Fig. 14 as a comparison of 350°C data obtained on CZ4 and CZ5 supported catalysts. Substantially greater CO_2 production and O_2 uptake, and correspondingly less CO breakthrough, is observed for the CZ4 catalyst, even though differences between the two catalysts in the long-pulse cycling experiments are less dramatic (500 μmol O/g for CZ4 vs. 460 μmol O/g for CZ5).

The CZ3 based catalyst, which showed the highest OSC at 350°C (570 μmol O/g) after 1050°C redox aging, was also redox aged at 1100°C and 1150°C. A slight fall-off in OSC (to 510 μmol O/g) was observed after 1100°C aging, but substantial deactivation (to 240 μmol O/g) was observed after 1150°C aging. The CZ2 based catalyst showed even more dramatic loss of OSC, from 390 μmol O/g after 1050°C aging to 90 μmol O/g after 1150°C aging. Note, however, that even after 1150°C redox aging, the catalysts prepared from CZ2 and CZ3 retained much greater OSC than the pure ceria based catalyst (C2) after 1050°C redox aging.

4. Discussion

Ten ceria-containing materials from Rhodia were characterized, covering the ceria-rich mixed oxide composition region from 66.5 to 99.5 wt% ceria and representing several proprietary processing schemes. The overall objective was to relate physical and chemical characteristics of the support materials to a measure of catalyst performance, namely OSC. To

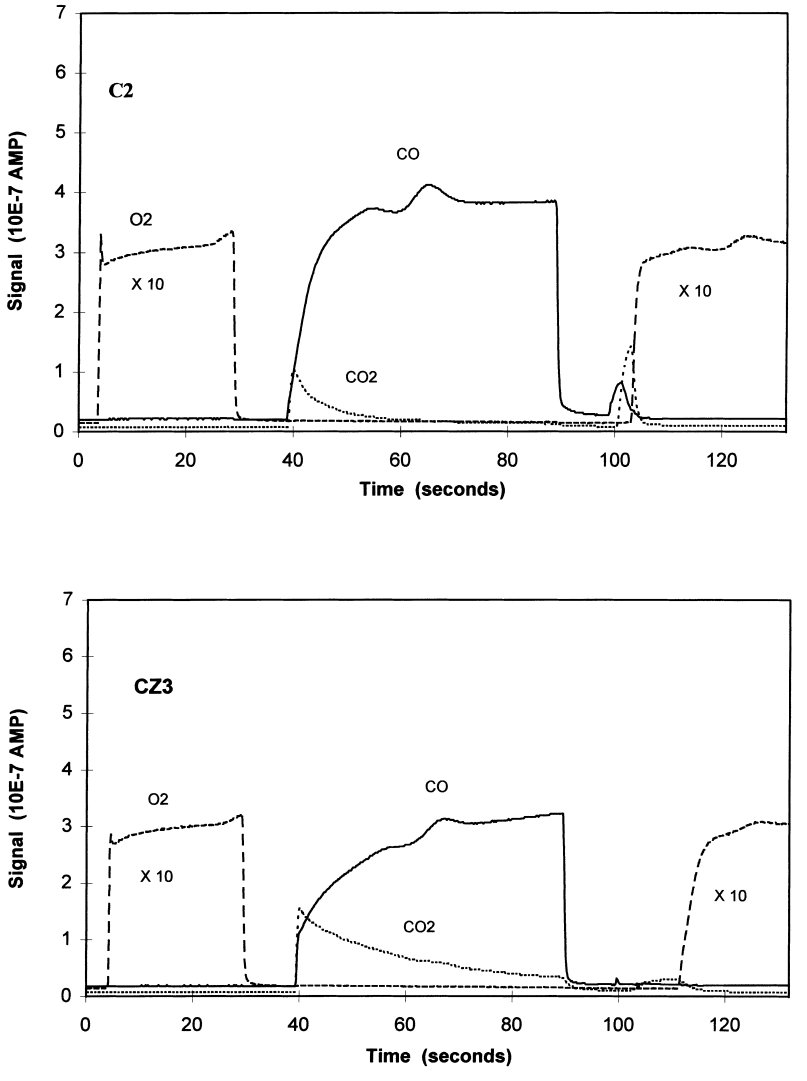

Fig. 11. Long-pulse OSC traces for fresh C2 (100% CeO_2) and CZ3 (70% CeO_2/30% ZrO_2) support materials (without Pd) at 500°C.

that end, this discussion focuses on the chief findings related to OSC, especially amongst the group of CZ(P) materials, since they are of greatest interest as automotive catalyst components.

OSC of the CZ1 material (90 wt% CeO_2–10 wt% ZrO_2) was intermediate between that of pure ceria and the ≈70% ceria materials. Its OSC was closer to that of the ≈70% ceria materials, in keeping with data of Cuif et al. [18] showing that the OSC increases rapidly with small additions of zirconia and reaches a maximum between 20 and 40 wt% zirconia in ceria.

The two ceria–zirconia support materials containing 5 wt% praseodymia (CZP1 and CZP2) were more stable than their undoped (70 wt% ceria–30 wt% zirconia) counterparts. In contrast to the CZ support materials, the CZP materials showed no phase segregation after 1050°C air aging and also retained equivalent or slightly higher BET areas after both redox and air aging. Despite the improved thermal stability, the OSC of the model catalysts supported on the CZP materials was no greater than that of the corresponding CZ catalysts. Photoemission spectra from the CZP

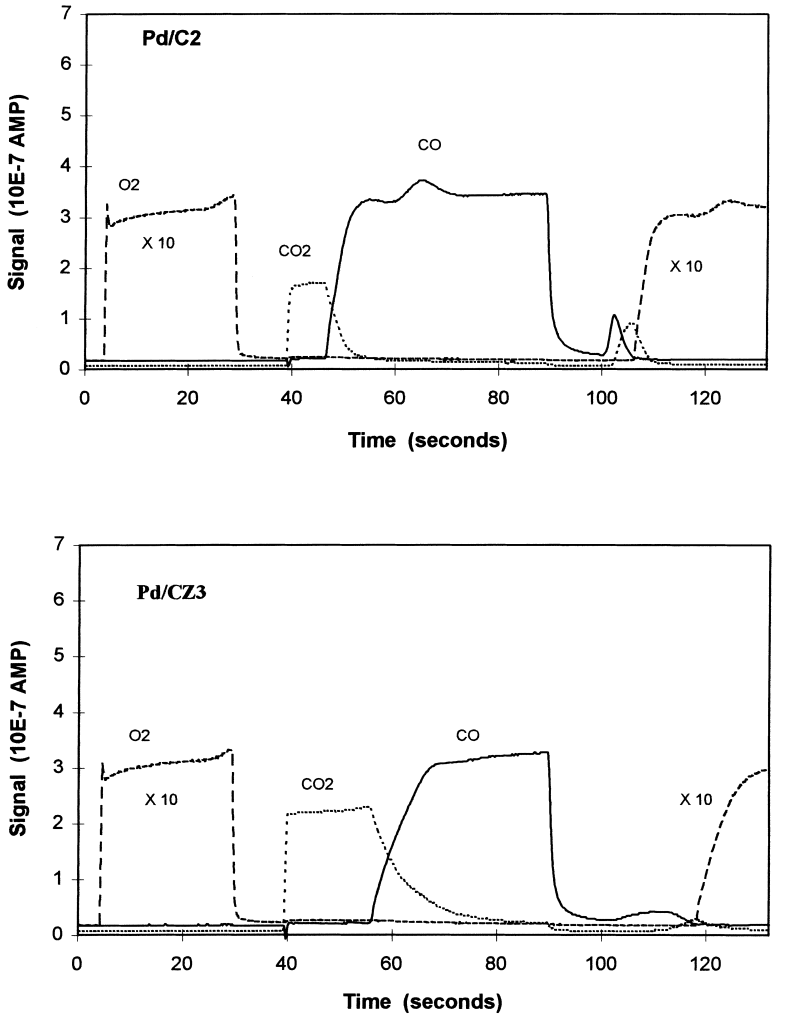

Fig. 12. Long-pulse OSC traces for fresh 2% Pd on C2 (100% CeO_2) and CZ3 (70% CeO_2/30% ZrO_2) support materials at 500°C.

materials (Fig. 9) indicate that Pr remains in the +3 oxidation state (i.e., reduced) even after extended oxidizing treatments at various temperatures. Thus, praseodymia, at the 5% level, acts as a stabilizer, much as the sesquioxides yttria and lanthana, but does not appear to undergo the cyclic redox between +3 and +4 necessary for OSC.

Among the CZ materials, the most interesting observation is the substantial differences in OSC obtained for the four 70/30 supports. These differences, for the most part, cannot be explained by the characterization data. No clear trends or distinguishing traits are observed in surface area stability, pore structure, ceria–zirconia phase composition, or temperature-programmed reduction characteristics among the model catalysts prepared on the 70/30 CZ supports. Furthermore, the XPS measurements, carried out separately on the same model catalysts, reveal factor-of-two differences in apparent Pd surface concentrations between the four 70/30 CZ supported catalysts after 1050°C redox aging (see Table 4). However, the differences do not follow the trends in OSC. The CZ2 and CZ3 supported catalysts, e.g., yield nearly identical apparent Pd surface concentrations despite showing the largest difference in OSC of the four 70/30 CZ formulations.

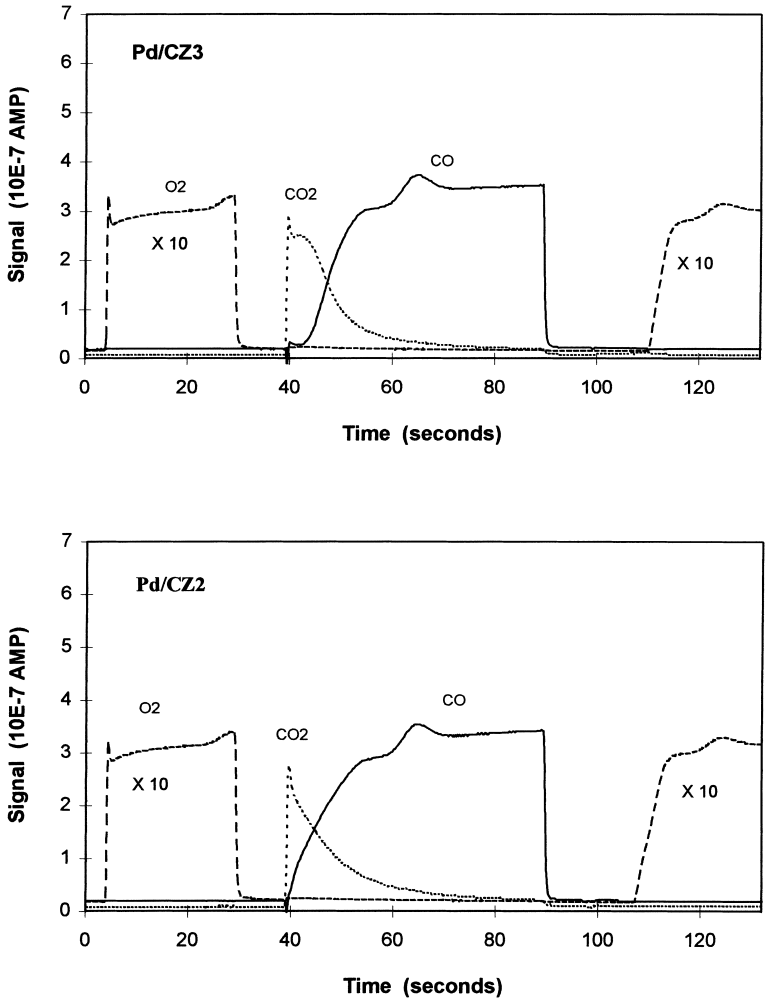

Fig. 13. Long-pulse OSC traces for 1050°C redox aged 2% Pd on CZ3 (70% CeO_2/30% ZrO_2) and CZ2 (70% CeO_2/30% ZrO_2) supports at 350°C.

Pd particle size estimates for the aged catalysts, obtained from both XPS (see Appendix A) and XRD, agree to within a factor of two and establish that Pd dispersion is a few percent at most, corresponding to particle diameters of ca. 20–40 nm. Given the large size of the Pd particles, and the lack of any correlation between particle size and OSC, the differences in OSC between the 70/30 CZ supported catalysts appear to be related to differences in the supports rather than in the Pd–support interaction. If so, the differences between supports must relate to differences in the ways the materials are processed and may be confined to spatial domains smaller than those probed by the conventional XRD employed in this study. Egami et al. [19] have suggested, from neutron diffraction data, that high-surface-area ceria–zirconia powders do indeed exhibit small-scale (i.e., nanometer) phase segregation.

The one distinguishing feature between the catalysts supported on CZ(P) materials and those on essentially pure ceria is the new peak in TPR which appears between 100°C and 200°C for the CZ(P) materials after 1050°C aging, but is totally absent in pure ceria. The peak is due to bulk reduction of ceria in solid solution, assisted by Pd. Interestingly, a peak in the same temperature range, attributed largely to bulk reduction of ceria, has been reported for

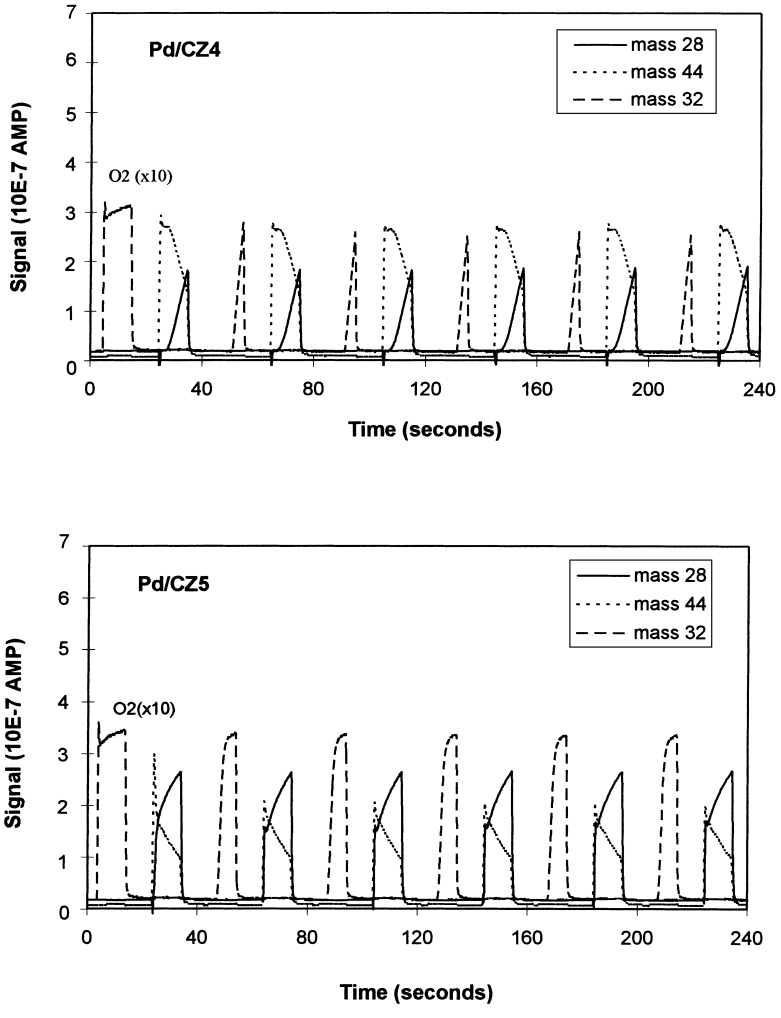

Fig. 14. Short-pulse OSC traces for 1050°C redox aged 2% Pd on CZ4 (70% CeO_2/30% ZrO_2) and CZ5 (70% CeO_2/30% ZrO_2) supports at 350°C. Mass 28 – CO; mass 44 – CO_2; mass 32 – O_2.

thermally aged Rh on $Ce_{0.5}Zr_{0.5}O_2$ [20]. The new peak represents an important mode of reduction because it accounts for a large fraction of the available oxygen (and presumably much of the OSC) in the aged catalysts. More fundamentally, it also explains why the ceria–zirconia supports are far superior to pure ceria in their retention of OSC after high-temperature aging. Once ceria loses surface area, its ability to supply oxygen from the bulk becomes limited at temperatures below ca. 800°C – far above normal TWC operating temperatures. The redox aged ceria–zirconia supports, on the other hand, retain their ability to rapidly supply oxygen from the bulk even at temperatures as low as 150°C.

The position and integrated area of the second peak provide a crude indication of the "goodness" of a Pd/CZ catalyst. This can be seen from changes in the peak as the aging temperature or aging environment is varied. Air aging at 1050°C retains the same peak position as redox aging at 1050°C but decreases the area. The OSC also decreases, and phase segregation is observed in XRD, indicating that the combined OSC of the two resulting phases is less than that of the single phase solid solution. In contrast, redox aging at

1150°C, compared to 1050°C, causes the second peak to shift to higher temperature without significantly changing the area. In this case, OSC also decreases, but no phase segregation is observed. Kinetic factors are likely to be controlling in this situation, with the higher aging temperature leading to larger Pd particles, larger ceria–zirconia grains, and lower rates of oxygen anion diffusion and/or insertion of surface vacancies.

5. Summary

- Pure ceria has poor surface area stability compared to solid solutions of ceria and zirconia, and retains little useful OSC after 1050°C aging.
- Silica-stabilized ceria shows good thermal stability in air but poor stability under hydrothermal aging conditions, thus precluding its applicability to automotive exhaust catalysis.
- Model catalysts consisting of 2% Pd on 70 wt% ceria–30 wt% zirconia supports retain large oxygen storage capacity (ca. 400–600 μmol O/g at 350°C) after 12 h, 1050°C redox aging. Low-temperature OSC decreases precipitously after 1150°C redox aging.
- Conventional catalyst characterization techniques do not discriminate between 70/30 Ce/Zr support materials prepared by different processes, although significant differences in OSC are observed for identically prepared model catalysts based on differently processed supports.
- Redox or air aging of model Pd-on-ceria/zirconia catalysts at 1050°C produces a TPR peak between 100°C and 300°C characteristic of Pd-assisted removal of oxygen from the ceria–zirconia bulk. This peak is absent for Pd-on-ceria catalysts.
- Ceria substitution in 70/30 Ce/Zr supports with 5 wt% praseodymia slightly improves the thermal stability of the ceria–zirconia but does not improve OSC, consistent with the XPS observation that Pr remains fixed in the +3 oxidation state.
- Surface analysis of the ceria–zirconia oxides by X-ray photoelectron spectroscopy shows no significant differences between surface and bulk Ce-to-Zr ratios, consistent with the view that the solid solutions prepared in this study are homogeneous materials.

Acknowledgements

C.L. Roe (Michigan Technological University) obtained the XPS data during a 1997 graduate summer internship at Ford. We also thank M. Aubert (Rhodia, La Rochelle, France) for preparing some of the supports.

Appendix A

Pd dispersion estimate from XPS

Assuming that all of the Pd particles in a given sample are of the same diameter, d, it is possible to estimate the Pd dispersion as follows: if N is the number of Pd atoms per cm^2 of support and n_d is the number of Pd particles of diameter d per cm^2 of support, then it follows that

$$fN = n_d(4/3)\pi(d^3/8)\rho(N_A/MW),$$

where ρ is the density (12 g/cm^3), MW is the atomic weight of Pd, and N_A is Avogadro's number. Further, if A is the fractional area of support covered by Pd particles, then

$$A = n_d\pi(d^2/4).$$

Eliminating n_d between these two relations leads to

$$N = 4A(4/3)(d/8)\rho(N_A/MW),$$

rewritten as

$$d = (N/A)(MW/N_A)/8.$$

But N is also known in terms of the Pd loading, L (0.02 g/g), and the specific surface area, A_s, i.e.,

$$N = (L/A_s)(N_A/MW).$$

Also, A is roughly equal to [Pd] in cases where d is greater than the photoelectron inelastic mean free path. For CZ3, the Pd particle size would thus be

$$d = ((0.02/74000)(N_A/MW)/(0.02))(MW/N_A)/8$$
$$= (1/74000)/8\,\text{cm} = 17\,\text{nm}.$$

This value, about a factor of two smaller than would be inferred from XRD line broadening, corresponds to a Pd dispersion of a few percent, which is typical of supported Pd catalysts.

References

[1] K.C. Taylor, Catal. Rev.-Sci. Eng. 35 (1993) 457.
[2] J.T. Kummer, J. Phys. Chem. 90 (1986) 4747.
[3] A. Trovarelli, Catal. Rev.-Sci. Eng. 38 (1996) 439.
[4] G.J. Bartley et al., Society of Automotive Engineers, Warrendale, PA, Paper no. 930076 (1993).
[5] B.H. Engler et al., Society of Automotive Engineers, Warrendale, PA, Paper no. 930738 (1993).
[6] J.C. Summers, J.J. White, W.B. Williamson, Society of Automotive Engineers, Warrendale, PA, Paper no. 890794 (1989).
[7] J.S. Hepburn et al., Society of Automotive Engineers, Warrendale, PA, Paper no. 941058 (1994).
[8] D.-J. Kim, J. Am. Ceram. Soc. 72 (1989) 1415.
[9] M. Yashima, H. Arashi, M. Kakihana, M. Yoshimura, J. Am. Ceram. Soc. 77 (1994) 1067.
[10] G.W. Graham, H.-W. Jen, W. Chun, R.W. McCabe, Catal. Lett. 44 (1997) 185.
[11] H.C. Yao, Y.F. Yu Yao, J. Catal. 86 (1984) 254.
[12] P. Fornasiero, G. Balducci, R. DiMonte, J. Kaspar, V. Sergo, G. Gubitosa, A. Ferrero, M. Graziani, J. Catal. 164 (1996) 173.
[13] G. Balducci, J. Kaspar, P. Fornasiero, M. Graziani, M.S. Islam, J. Phys. Chem. B 102 (1998) 557.
[14] G. Balducci, J. Kaspar, P. Fornasiero, M. Graziani, M.S. Islam, J.D. Gale, J. Phys. Chem. B 101 (1997) 1750.
[15] C.E. Hori, H. Permana, K.Y.S. Ng, A. Brenner, K. More, K. Rahmoeller, D. Belton, Appl. Catal. B 16 (1998) 105.
[16] G. Chen, W.T. Chon, C. Yeh, Appl. Catal. 8 (1983) 389.
[17] M.Yu. Sinev, G.W. Graham, L.P. Haack, M. Shelef, J. Mater. Res. 11 (1996) 1960.
[18] J.-P. Cuif et al., Society of Automotive Engineers, Warrendale, PA, Paper no. 970463 (1997).
[19] T. Egami, W. Dmowski, R. Brezny, Society of Automotive Engineers, Warrendale, PA, Paper no. 970461 (1997).
[20] P. Fornasiero, J. Kaspar, M. Graziani, J. Catal. 167 (1997) 576.